Extreme Mechanics Letters 28 (2019) 76–80

Contents lists available at ScienceDirect

Extreme Mechanics Letters

journal homepage: www.elsevier.com/locate/eml

Programmable elastic valley Hall insulator with tunable interface propagation routes

Quan Zhang, Yi Chen, Kai Zhang, Gengkai Hu *

Key Laboratory of Dynamics and Control of Flight Vehicle, Ministry of Education, School of Aerospace Engineering, Beijing Institute of Technology, Beijing 100081, China

A R T I C L E   I N F O

Article history:
Received 28 December 2018
Received in revised form 25 January 2019
Accepted 12 March 2019
Available online 15 March 2019

Keywords:
Elastic topological insulator
Programmable interface propagation route
Topologically protected edges wave
Wave guiding

A B S T R A C T

A challenge in the area of topologically protected edge waves in elastic media is how to tune the topological interface propagation route as needed. This paper proposes a tunable elastic valley Hall insulator, whose unit cell consists of two cavities and magnetic fluid with the same volume as the cavity. Interface route with arbitrary shape for propagating topologically protected edge waves can be achieved by controlling the distribution of magnetic fluid in each unit cell through a designed programmable magnet lifting array. As demonstrated through numerical simulations and experimental testing, the flexural wave is confined to propagate along the topological interface routes of different configurations. Finally, it is indicated that the proposed valley Hall insulator can be applied to achieve desired localized elastic energy which is robust to defects, sharp corners and so on.

1. Introduction

During the past decades, manipulating wave propagation in periodic materials has attracted significant interest. Many exciting functions such as wave guiding, negative refraction, focusing and even cloaking have been conceived through the engineering of band structure. Recently, the advent of topological mechanics, originated from quantum systems of condensed matter [1], has attracted researchers to exploit the topological properties of band structure. One of the most famous feature is that the domain walls between materials with distinct topological indices support edge waves, which are topologically protected against defects and sharp corners [2]. This concept has been quickly extended to other classic physical areas such as photonics [3–8], acoustics [9–15] and mechanics [16–18].

Realization of topologically protected edge waves (TPEWs) in acoustic and mechanical systems is attractive due to its promising perspectives such as high-efficiency wave guiding. By mimicking the quantum Hall effect (QHE) [1], quantum spin Hall effect (QSHE) [19,20] and quantum valley Hall effect (QVHE) [21] in quantum systems, three broad ways have been achieved to realize TPEWs in acoustic/elastic media, which are called acoustic/elastic quantum Hall effect [11–14], acoustic/elastic quantum "pseudo-spin" Hall effect [22–25] and acoustic/elastic valley Hall effect [26–34], respectively. Generally, in topological materials based on QHE, external field interacting with the wave medium is needed to break time-reversal symmetry (TRS). In acoustic/elastic system, the mostly common used method to break TRS is by exploiting rotating inclusions, such as spinning rotors [12,14] or fluids [11,13]. Compared to QHE, the QSHE and QVHE have advantages in practical applications since the topological materials based on QSHE and QVHE do not need external field. Both the QHE and QSHE enable the realization of unidirectional TPEWs while the QVHE does not. Moreover, the TPEWs in topological system based on QVHE are easier to be scattered by lattice scale defects compared with that based on QHE and QSHE. However, the QSHE based-designs often result in nontrivial geometric or material configurations in order to engineer the band structure that requires a finely double Dirac cone [34]. The QVHE, relies only on breaking the space-inversion symmetry, which is relatively easier to achieve in elastic systems of practical interest. Currently, most studies are focused on designing the microstructure to realize a type of TPEWs. In future practical applications, it is required to guide wave propagation on different topological interface routes in the same piece of periodic media. In acoustic system, realizations of tunable topological edge states are of current research interest. Reconfigurable topological edge states have been achieved by controlling the size or the orientation angle of the scatterers [24,33]. In elastic system, studies reporting on the experimental observation of reconfigurable topological edge states in continuous elastic media are still quite limited. Our work is aimed to realize experimentally tunable interface routes for propagating TPEWs in elastic system.

Recently, a type of tunable elastic metamaterial — called "tunable fluid–solid composite" is reported, which enables the realization of tunable locally resonant band gap [35]. Inspired by

* Corresponding author.
E-mail address: hugeng@bit.edu.cn (G. Hu).

https://doi.org/10.1016/j.eml.2019.03.002
2352-4316/

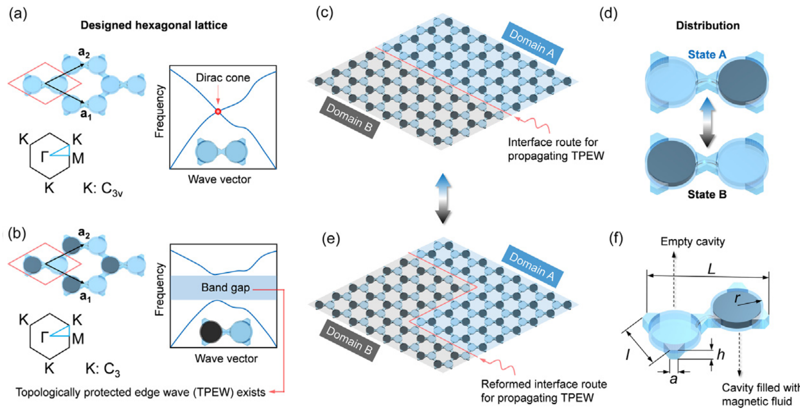

Fig. 1. Designed tunable valley Hall insulator. (a) Each unit cell of the designed hexagonal lattice consists of two cylindrical cavities. The dispersion diagram of the lattice features K-point Dirac cone. (b) The Dirac cone is broken to form a band gap when one cavity of the unit cell is filled with magnetic fluid. (c) For frequency located in the band gap, topologically protected edge state exists along the interface between two pieces of insulators characterized by distinct topologies. (d) The magnetic fluid can be transferred between the pair of cavities in each unit cell through a designed programmable magnetic potential. (e) The shape of the interface route for propagating TPEWs can be easily tuned since the mass distribution in each unit cell can be modified. (f) Geometric parameters of the designed unit cell.

this work, here we report a tunable elastic lattice that contains both solid and liquid materials (magnetic fluid). By using programmable external magnetic potential, the distribution of magnetic fluid in each unit cell can be modified independently. This allows the formation of topological interface route with programmable arbitrary shape in the elastic lattice by exploiting valley degrees of freedom.

2. Results

To achieved TPEWs in a periodic system by mimicking quantum valley Hall effect, the unit cell should satisfy C_3 symmetry and violate inversion symmetry [26,28]. As shown in Fig. 1a, each unit cell of the designed hexagonal lattice consists of two cylindrical cavities, which are connected to each other through a small arched channel. It is obvious that the lattice satisfies C_3 symmetry and inversion symmetry simultaneously. Correspondingly, the dispersion diagram features K-point Dirac cone since the corner points possess C_{3v} symmetry. In order to break the inversion symmetry of the lattice, magnetic fluid with the volume that just enough to fully fill one cavity is injected into the unit cell. When the magnet fluid is attracted into one cavity, the localized liquid breaks the inversion symmetry of the lattice. Therefore, the Dirac cone is broken to form a band gap since the corner points only possess C_3 symmetry (Fig. 1b). For frequency located in the band gap, TPEW exists along the interface between two pieces of insulators characterized by distinct topologies, as shown in Fig. 1c. Meanwhile, a magnet lifting array is designed to create a programmable magnetic potential, which allows independent tuning of the magnetic fluid distribution in each unit cell (Fig. 1d). Therefore, the distribution state of magnetic fluid in any block region of domain A can be transformed into that in domain B and vice versa. As a result, the interface route for propagating TPEWs can be easily tuned (Fig. 1e).

To verify the designed valley Hall interface states, we focus on the elastic lattice shown in Fig. 1. The material parameters for the whole lattice plate are Young's modulus $E = 2$ GPa, density $\rho = 1200$ kg m^{-3}, respectively, and Poisson's ratio is assumed to be 0.4. The geometric parameters are illustrated in Fig. 1f, where the unit cell size L is 4 cm; $l = 1.866$ cm; $a = L{-}2l$; the thickness of lattice plate is $h = 4.0$ mm; the outer radius and wall thickness of cylindrical cavities are 8.6 mm and 0.7 mm, respectively.

We firstly calculate the band structures for the unit cells. In the simulation, we use the Acoustic-Solid Interaction module in COMSOL Multiphysics to calculate the Eigen frequencies for any given wave vector located on the irreducible Brillouin zone (IBZ). Acoustic parameters for modeling magnetic fluid are $\rho_{MF} = 1100$ kg m^{-3} and $c_{MF} = 1400$ m s^{-1}. In the relatively low frequency range, where the acoustic wavelength in the liquid medium is much larger than the size of the cavity, the acoustic velocity of the liquid has no influence on the numerical results (Supplementary Material). Fig. 2a shows the dispersion relation of the referenced unit cell without magnetic fluid. The dispersion branches that correspond to out-of-plane and in-plane polarized modes are separated from each other, shown with blue and orange lines respectively. A Dirac cone is observed on the out-of-plane branches at K point of the first Brillouin zone, since the lattice satisfies space-inversion symmetry. However, once magnetic fluid fully fills one cavity of the unit cell, the localized liquid will break the space-inversion symmetry, which opens the Dirac cone to form a band gap with the frequency range from 1226 Hz to 1440 Hz (Fig. 2b).

In addition to the case that magnetic fluid is completely concentrated in one cavity, the width of the topological band gap can be continuously tuned under different liquid distribution states. Assuming that the masses of magnetic fluid in the left and right cavities of the unit cell are m_1 and m_2, respectively. Meanwhile, the sum of m_1 and m_2 (the total mass of magnetic fluid in each unit cell) is kept constant. A dimensionless parameter $m = (m_1 - m_2) / (m_1 + m_2)$ is defined to present the distribution state of magnetic fluid. For instance, $m = +1$ and $m = -1$ correspond to the cases that magnetic fluid is concentrated in the left cavity and right cavity, respectively. Fig. 2c shows the variation of the band-edge frequencies at K as a function of m. We can see that the gap width is monotonically increasing as the absolute value of m increases. Moreover, the band gap closes at $m = 0$ and is symmetry about $m = 0$. The eigenvectors $\boldsymbol{\psi}$ (where the subscript represents the value of m) that correspond to band-edge frequencies for $m = +1$ and $m = -1$ are presented in Fig. 2d, which illustrates the phenomenon of band inversion. Although the band-edge frequencies are preserved under the transformation $m \to -m$ due to time-reversal symmetry, the eigenvectors with the same frequency feature opposite polarizations. For instance, the eigenvector of the first (second) mode is clockwise (counterclockwise) polarized for $m = -1$, while the opposite is observed for $m = +1$. This chirality revolution at each valley (i.e., clockwise and anticlockwise) plays the role of the valley degree of freedom [26]. The change in polarization across $m = 0$ suggests that lattices with $m > 0$ and $m < 0$ have opposite valley Chern numbers, which is the integral of the Berry curvature over

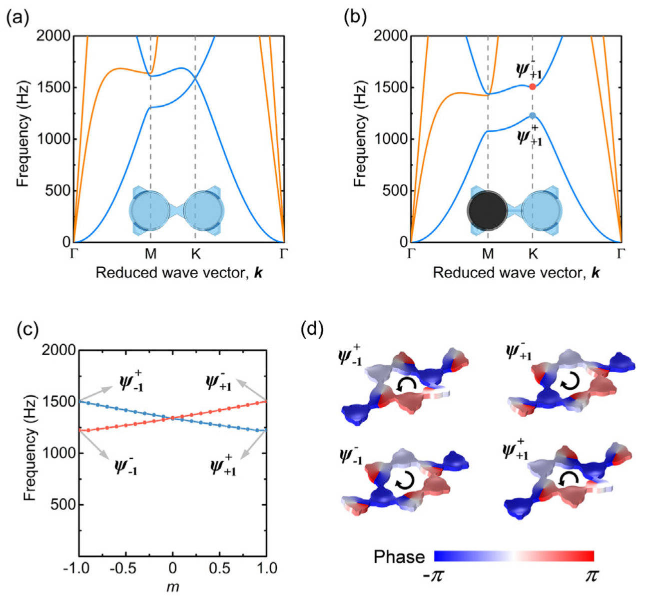

Fig. 2. Dispersion analysis. (a) A Dirac cone exists in the referenced lattice. (b) The Dirac cone is opened to form a band gap once magnetic fluid fully fills one cavity of the unit cell. (c) Variation of the band-edge frequencies at K as a function of m. (d) The eigenvectors of the first two out-of-plane modes at K for $m = -1$ and $m = 1$. (For interpretation of the references to color in this figure legend, the reader is referred to the web version of this article.)

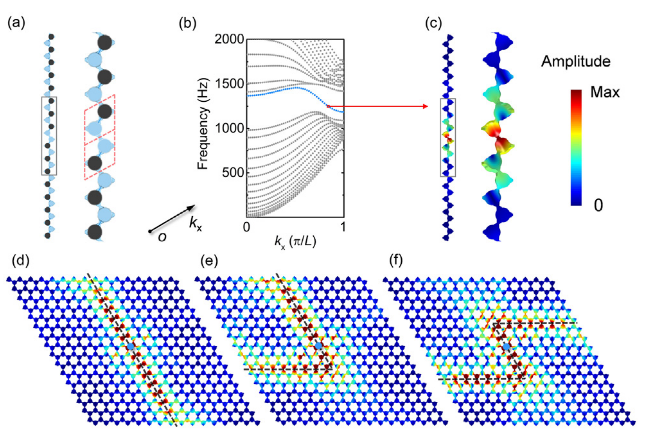

Fig. 3. Numerical analysis of the topological interface propagation states. (a) The FE model of the super cell. (b) Out-of-plane polarized branches of the strip, the blue dot line represents the interface mode. (c) Eigenvector corresponding to the interface mode evaluated at $f = 1234$ Hz. (d–f) The calculated displacement fields at $f = 1234$ Hz for the straight-line, L-shape and Z-shape interface configurations, respectively.

half the Brillouin zone [28]. By using the efficient method for calculating Chern number on a discretized Brillouin zone [36], we carried out the numerical calculation of the valley Chern number at K point. For instance, the calculated valley Chern number of the first flexural mode is about $+0.2$ for $m = 0.5$. When m is changed to be -0.5, the corresponding valley Chern number is inverted to be -0.2. We can see that the calculated values show a huge difference from the theoretical quantized value $C_v = \pm 0.5$. This discrepancy is due to the strong breaking of space inversion symmetry [34]. To demonstrate this assertion, we also calculated the valley Chern numbers at K point of the first mode for $m = \pm 0.1$(weaker breaking of space inversion symmetry). The resulting valley Chern numbers are ± 0.45, which is very close to the theoretical value.

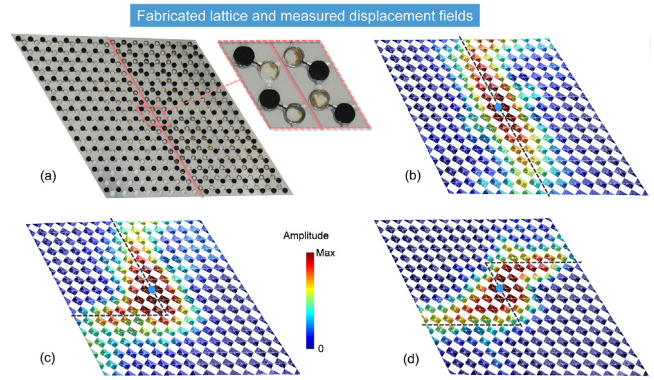

Fig. 4. Experimental demonstration of the tunable topological interface routes for propagating TPEWs. (a) The fabricated lattice sample. (b–d) The measured displacement fields for the straight-line, L-shape and Z-shape interface configurations, respectively.

Next, to demonstrate the existence of interface modes, the dispersion relations of a strip including 16 unit cells and an interface (Fig. 3a) is analyzed. Fig. 3b shows the out-of-plane polarized dispersion branches of the strip. Among these out-of-plane modes, an interface mode is observed shown in blue dot line. For instance, one eigenvector corresponding to the interface mode is illustrated in Fig. 3c, where the displacement field localizes at the interface and decays rapidly away from it. The dispersion analysis indicates that topologically protected interface modes associated with out-of-plane elastic wave can be achieved in the designed elastic lattice.

We further carry out frequency domain simulations about the propagations of TPEWs. In the simulations, the Low-Reflecting Boundary condition in COMSOL is assigned to the external boundaries of the lattice and an out-of-plane harmonic excitation at 1234 Hz is applied at the position shown with blue circle. The simulated straight-line interface propagation state is shown in Fig. 3d, the distribution of magnet fluid in unit cells on the left side of the interface is exact opposite with that in unit cells on the right side of the interface. Fig. 3d illustrates that the excited out-of-plane wave propagates along the interface and has limited penetration into the bulk. When the interface route is changed to be L-shape or Z-shape, the harmonic excitation with the same frequency travels along the newly formed interface with a limited propagation into the bulk (Fig. 3e, f).

To validate the theoretical and numerical predictions, as shown in Fig. 4a, a lattice sample consisting 16 × 16 unit cells is fabricated by using a three-dimensional (3D) printer (Object 350, Stratasys, USA) with a photosensitive resin (RGD810, Veroclear, Stratasys, USA). The fabricated sample is then placed on a cardboard and a continuous out-of-plane harmonic excitation is applied at the center of the sample, as shown in Supplementary Fig. S2. The resulting wave propagation field is recorded using a scanning laser Doppler vibrometer (PSV-400, Polytec GmbH, Germany). Three typical interface configurations: straight-line route, L-shape route and Z-shape route are achieved by controlling magnetic fluid distribution in the corresponding unit cells through a designed magnet lifting array, which can be controlled by a programmed computer software (Supplementary Fig. S3). The process for controlling magnetic fluid distribution to form a specific interface route through the magnet lifting array is shown in Supplementary Video.

The experimental root mean squared distributions of the velocity field at 1450 Hz for structure configuration with straight-line interface route is shown in Fig. 4b. The exciting position and the interface route are highlighted as the blue circle and the

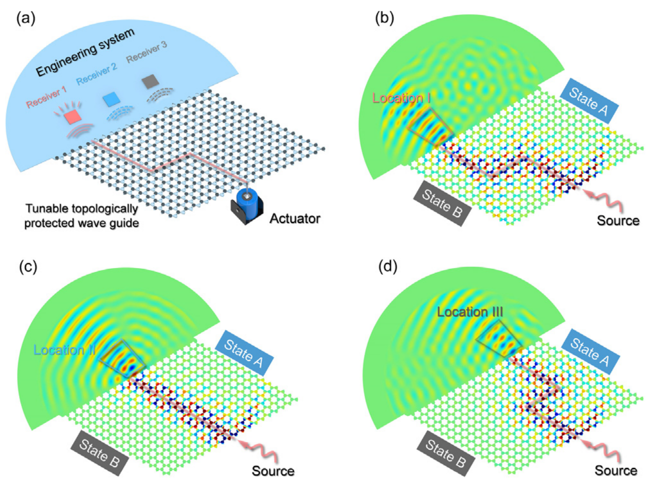

Fig. 5. Demonstration of tunable wave guiding functions based on the proposed valley Hall insulator. (a) The implementation of applying the tunable valley Hall insulator to an engineering system that requires localized elastic energy. (b-d) Simulation results about guiding elastic energy to arrive at different target regions.

black dot line, respectively. We can see that the induced out-of-plane wave travels along the interface and decays rapidly in the direction perpendicular to the interface. Moreover, obvious edge state is observed on the right half of top side, which can be explained by simulating the displacement field of the lattice under free boundary conditions, as shown in Supplementary Material. When the magnetic fluid distribution is changed through the magnet lifting array to form a L-shape or Z-shape interface route, the measured flexural wave fields are shown in Fig. 4c, d. The results indicate that the wave excited at the same position propagates along the newly formed topological interface with limited propagation into the bulk. The flexural wave turns its direction for 120° at the corner with limited backscattering. The measured wave field shows visible decay along the interface, this is mainly due to the large material damping of the used 3D printed photosensitive resin. To demonstrate it, we calculate the displacement fields with the effect of material damping of the printed photosensitive resin, as shown in Supplementary Fig. S7. Obvious decay along the interface route can be observed. In addition, we also measured the displacement fields for other frequencies located in the topological band gap. As shown in Supplementary Fig. S8, the valley protected interface propagations still exist. It should be noted that the selected experimental testing frequencies are slightly beyond the predicted band gap. This is resulted from the geometric error caused by 3D printing and effect of the glue used to seal the cavities.

In acoustic valley Hall insulators, it has been proven that the sharp bends induce very little backscattering [26,33]. Likewise, in our proposed tunable elastic valley Hall insulator, both the experimental and simulated results indicate that the sharp bends induce limited backscattering. Moreover, we measured the displacement field after importing a small defect formed by destructing the magnetic fluid distribution in two unit cells on the interface path. As shown in Supplementary Fig. S9, we can see that the elastic wave detouring around the small defect while maintaining nearly a loss-free elastic transmission. Although lattice-scale defects usually induce strong backscattering [33], the proposed valley Hall insulator is robust to the disorderly distribution of magnetic fluid in very few unit cells.

3. Discussion

Phononic crystals and elastic metamaterials have excellent performances in manipulating elastic waves compared to traditional materials [37,38]. Moreover, tunable elastic metamaterials have been achieved [38–41], which enables guiding elastic energy to arrive at different local regions under different working conditions. However, a major shortcoming is that elastic waves guided by metamaterials can be easily scattered or localized by bends and defects [12], which makes the transfer efficiency for elastic energy greatly reduced. In comparison, our proposed tunable elastic valley Hall insulator can address this issue due to the topological protection effect. For instance, Fig. 5 illustrates that our proposed tunable valley Hall insulator can serve as a smart wave guide that allows delivering elastic energy to different receivers in an engineering system. In the implementation, the actuator and the engineering system is connected through the proposed tunable valley Hall insulator, as shown in Fig. 5a. When receiver 1 requires elastic energy while the other ones do not need it under a specific operating mode, the wave guide that connects the actuator and the local region near receiver 1 can be formed by controlling the magnetic fluid distributions. As expected, the elastic energy accurately arrives at the local area where receiver 1 is located with limited impact on the other receivers (Fig. 5b). When the operating mode is switched in the engineering system, correspondingly, the topological wave guide is tuned to ensure that elastic energy only reaches the target region (Fig. 5c, d). Compared to previous topological insulators and tunable metamaterials, our proposed tunable elastic valley Hall insulator has advantages in designing intelligent elastic waveguide with high transfer efficiency in practical applications.

4. Conclusions

In summary, we proposed a type of tunable elastic valley Hall insulator, each unit cell of which consists of two cavities and a certain volume of magnetic fluid. Interface route with arbitrary shape for propagating TPEWs can be achieved by controlling the magnetic fluid distribution in each unit cell through a designed programmable magnet lifting array. Experiments are conducted to validate the propagations of TPEWs along three interface routes: straight-line, L-shape and Z-shape. In each interface configuration, the induced flexural wave propagates along the topological interface with a limited propagation into the bulk. The proposed programmable valley Hall insulator provides a perspective for the design of tunable intelligent elastic waveguide that is robust to small defects and sharp corners.

Acknowledgments

This work was supported by the National Natural Science Foundation of China [Grants No. 11632003 and No. 11672037]. The authors thank Prof. L.Z., Y.J. and C.J. for help in experiments.

Appendix A. Supplementary data

Supplementary material related to this article can be found online at https://doi.org/10.1016/j.eml.2019.03.002.

References

[1] F.D. Haldane, Model for a quantum hall effect without landau levels: Condensed-matter realization of the parity anomaly, Phys. Rev. Lett. 61 (1988) 2015–2018.

[2] Y. Chen, X. Liu, G. Hu, Topological phase transition in mechanical honeycomb lattice, J. Mech. Phys. Solids 122 (2019) 54–68.

[3] F.D. Haldane, S. Raghu, Possible realization of directional optical waveguides in photonic crystals with broken time-reversal symmetry, Phys. Rev. Lett. 100 (2008) 013904.

[4] Z. Wang, Y.D. Chong, J.D. Joannopoulos, M. Soljacic, Reflection-free one-way edge modes in a gyromagnetic photonic crystal, Phys. Rev. Lett. 100 (2008) 013905.

[5] Z. Wang, Y. Chong, J.D. Joannopoulos, M. Soljacic, Observation of unidirectional backscattering-immune topological electromagnetic states, Nature 461 (2009) 772–775.

[6] L. Lu, J.D. Joannopoulos, M. Soljačić, Topological photonics, Nat. Photon 8 (2014) 821–829.

[7] K.Y. Bliokh, F.J. Rodríguez-Fortuño, F. Nori, A.V. Zayats, Spin–orbit interactions of light, Nat. Photon 9 (2015) 796–808.

[8] A.B. Khanikaev, G. Shvets, Two-dimensional topological photonics, Nat. Photon 11 (2017) 763–773.

[9] E. Prodan, C. Prodan, Topological phonon modes and their role in dynamic instability of microtubules, Phys. Rev. Lett. 103 (2009) 248101.

[10] L. Zhang, J. Ren, J.S. Wang, B. Li, Topological nature of the phonon Hall effect, Phys. Rev. Lett. 105 (2010) 225901.

[11] A.B. Khanikaev, R. Fleury, S.H. Mousavi, A. Alu, Topologically robust sound propagation in an angular-momentum-biased graphene-like resonator lattice, Nature Commun. 6 (2015) 8260.

[12] P. Wang, L. Lu, K. Bertoldi, Topological phononic crystals with one-way elastic edge waves, Phys. Rev. Lett. 115 (2015) 104302.

[13] Z. Yang, F. Gao, X. Shi, X. Lin, Z. Gao, Y. Chong, B. Zhang, Topological acoustics, Phys. Rev. Lett. 114 (2015) 114301.

[14] L.M. Nash, D. Kleckner, A. Read, V. Vitelli, A.M. Turner, W.T. Irvine, Topological mechanics of gyroscopic metamaterials, Proc. Natl. Acad. Sci. USA 112 (2015) 14495–14500.

[15] C. He, Z. Li, X. Ni, X.C. Sun, S.Y. Yu, M.H. Lu, X.P. Liu, Y.F. Chen, Topological phononic states of underwater sound based on coupled ring resonators, Appl. Phys. Lett. 108 (2016) 031904.

[16] C.L. Kane, T.C. Lubensky, Topological boundary modes in isostatic lattices, Nat. Phys. 10 (2013) 39–45.

[17] J. Paulose, A.S. Meeussen, V. Vitelli, Selective buckling via states of self-stress in topological metamaterials, Proc. Natl. Acad. Sci. USA 112 (2015) 7639–7644.

[18] R. Susstrunk, S.D. Huber, Observation of phononic helical edge states in a mechanical topological insulator, Science 349 (2015) 47–50.

[19] B.A. Bernevig, T.L. Hughes, S.C. Zhang, Quantum spin Hall effect and topological phase transition in HgTe quantum wells, Science 314 (2006) 1757–1761.

[20] C.L. Kane, E.J. Mele, Quantum spin Hall effect in graphene, Phys. Rev. Lett. 95 (2005) 226801.

[21] D. Xiao, W. Yao, Q. Niu, Valley-contrasting physics in graphene: magnetic moment and topological transport, Phys. Rev. Lett. 99 (2007) 236809.

[22] S.H. Mousavi, A.B. Khanikaev, Z. Wang, Topologically protected elastic waves in phononic metamaterials, Nature Commun. 6 (2015) 8682.

[23] C. He, X. Ni, H. Ge, X.C. Sun, Y.B. Chen, M.H. Lu, X.P. Liu, Y.F. Chen, Acoustic topological insulator and robust one-way sound transport, Nat. Phys. 12 (2016) 1124–1129.

[24] J.P. Xia, D. Jia, H.X. Sun, S.Q. Yuan, Y. Ge, Q.R. Si, X.J. Liu, Programmable coding acoustic topological insulator, Adv. Mater. 30 (2018) 1805002.

[25] S.Y. Yu, C. He, Z. Wang, F.K. Liu, X.C. Sun, Z. Li, H.Z. Lu, M.H. Lu, X.P. Liu, Y.F. Chen, Elastic pseudospin transport for integratable topological phononic circuits, Nature Commun. 9 (2018) 3072.

[26] J. Lu, C. Qiu, L. Ye, X. Fan, M. Ke, F. Zhang, Z. Liu, Observation of topological valley transport of sound in sonic crystals, Nat. Phys. 13 (2016) 369–374.

[27] R.K. Pal, M. Ruzzene, Edge waves in plates with resonators: an elastic analogue of the quantum valley Hall effect, New J. Phys. 19 (2017) 025001.

[28] J. Vila, R.K. Pal, M. Ruzzene, Observation of topological valley modes in an elastic hexagonal lattice, Phys. Rev. B 96 (2017).

[29] M. Yan, J. Lu, F. Li, W. Deng, X. Huang, J. Ma, Z. Liu, On-chip valley topological materials for elastic wave manipulation, Nature Mater. 17 (2018) 993–998.

[30] Z. Zhang, Y. Tian, Y. Wang, S. Gao, Y. Cheng, X. Liu, J. Christensen, Directional acoustic antennas based on valley-hall topological insulators, Adv. Mater. (2018) 1803229.

[31] X. Wen, C. Qiu, J. Lu, H. He, M. Ke, Z. Liu, Acoustic dirac degeneracy and topological phase transitions realized by rotating scatterers, J. Appl. Phys. 123 (2018) 091703.

[32] M. Wang, L. Ye, J. Christensen, Z. Liu, Valley physics in non-hermitian artificial acoustic boron nitride, Phys. Rev. Lett. 120 (2018) 246601.

[33] Z. Zhang, Y. Tian, Y. Cheng, Q. Wei, X. Liu, J. Christensen, Topological acoustic delay line, Phys. Rev. Appl. 9 (2018) 034032.

[34] H. Zhu, T.W. Liu, F. Semperlotti, Design and experimental observation of valley-Hall edge states in diatomic-graphene-like elastic waveguides, Phys. Rev. B. 97 (2018) 174301.

[35] Q. Zhang, K. Zhang, G. Hu, Tunable fluid-solid metamaterials for manipulation of elastic wave propagation in broad frequency range, Appl. Phys. Lett. 112 (2018) 221906.

[36] T. Fukui, Y. Hatsugai, H. Suzuki, Chern numbers in discretized brillouin zone: Efficient method of computing (spin) hall conductances, J. Phys. Soc. Japan 74 (2005) 1674–1677.

[37] Y. Liu, Z. Liang, F. Liu, O. Diba, A. Lamb, J. Li, Source illusion devices for flexural lamb waves using elastic metasurfaces, Phys. Rev. Lett. 119 (2017) 034301.

[38] Z. Wang, Q. Zhang, K. Zhang, G. Hu, Tunable digital metamaterial for broadband vibration isolation at low frequency, Adv. Mater. 28 (2016) 9857–9861.

[39] A. Bergamini, T. Delpero, L.D. Simoni, L.D. Lillo, M. Ruzzene, P. Ermanni, Phononic crystal with adaptive connectivity, Adv. Mater. 26 (2014) 1343–1347.

[40] P. Wang, F. Casadei, S. Shan, J.C. Weaver, K. Bertoldi, Harnessing buckling to design tunable locally resonant acoustic metamaterials, Phys. Rev. Lett. 113 (2014) 014301.

[41] Q. Zhang, D. Yan, K. Zhang, G. Hu, Pattern transformation of heat-shrinkable polymer by three-dimensional (3D) printing technique, Sci. Rep. 5 (2015) 8936.